



Nuclear Materials Authority
P.O.Box 530 Maadi, Cairo, Egypt

ISSN 2314-5609
Nuclear Sciences Scientific Journal
8, 117- 140
2019
<http://www.ssnma.com>

MINERALOGY AND RADIOACTIVITY STUDIES OF WADI ABU HAMUR-SAFAGA STREAM SEDIMENTS, CENTRAL EASTERN DESERT, EGYPT

ASHRAF EL AZAB
Nuclear Materials Authority, Cairo, Egypt

ABSTRACT

The studied area covered by igneous and metamorphic rocks represented by Metagabbro, Metavolcanic, Older Granite, Dokhan Volcanics, Hammamat Sediments, and Younger Granite. Faults are essential structural features in the study area. The strike-slip faults of NW trends are right-lateral, while those of E-W, NE, and NNE trends are left-lateral faults. The normal faults are only preserved on a minor scale along these strike-slip faults represented by nearly vertical slicken-sides that indicate substantial vertical displacement.

The grain size analysis and its distribution is a fundamental descriptive measure of clastic sediments. The results of statistical parameters a graphic mean (M_z) ranging from 0.04ϕ to 1.8ϕ , which means that it lies in coarse and medium sand size classes represented by 70% and 30%, respectively; inclusive graphic standard deviation (σ_i) ranging from 0.88 to 1.8. The samples could be categorized in the poorly sorted class and moderately sorted represented by 75% and 25%, respectively; inclusive graphic Skewness (Sk_i) ranging from 0.03 to 0.33, the samples could be categorized in fine skewed, near symmetrical, and strongly fine skewed classes represented by 55%, 40%, and 5%, respectively. Inclusive graphic Kurtosis (K_g) ranging from 0.68 to 2.05, the samples could be categorized in the platykurtic; mesokurtic, very leptokurtic and leptokurtic classes represented by 35%, 25%, 15% and 25%, respectively.

The average content of total heavy minerals is 4.5% while the heavy content is ranging from 2% and 10.5%. Opaque minerals represented by magnetite, hematite, ilmenite constituents have an average of 1.07%, 0.1%, and 0.286%, respectively. Abrasive minerals as garnet constituents has an average of 0.13%, and pigment minerals as rutile and titanite constituents have an average of 0.188%, and 0.23%, respectively. Radioactive minerals as fluorites, zircon, and thorite constituents have an average of 0.0075%, 0.184%, and 0.001%, respectively. Amphiboles and pyroxene constituents range from 0.1% to 3.78% with an average of 2.22%. The eU contents range between 1 and 4ppm with an average of 1.76ppm, while eTh is between 2 and 29 ppm with an average of 10.75ppm. The average Ra average content for these sediments is 2.89 ppm, while the average content of K% is 1.16%.

INTRODUCTION

The study area represented by wadi abu hamur-wadi safaga which has long 30km and width reach to 50m (Fig.1). These wadis lies roughly south of the Safaga-Qena road in unpaved road about 10km. The study area

is bordered to the east by the Tertiary clastics and Cretaceous phosphatic deposits of Wadi Muhammad Rabah. The area are characterized by high rugged topographic area includes different mountains as G. um tagher, G. abu furad, G. wairah and G. muhammad rabah. The area in upstream reaches to 700m

continental crust were partly based on a study of this area by Akaad et al. (1973). Detailed regional studies have also been completed by El-Gaby and Habib (1980, 1982).

In the following description of the rock units of the area according to the Geological map of Abd El Rahman Fowlar et. Al., 2006, (Fig.1).

GEOLOGIC SETTING

Metagabbro

It is present in central part of wadi Abu Hamur and the end of wadi safaga. A wide strip of green-schist facies metamorphosed weakly deformed gabbro.

Massive to weakly deformed gabbro, and form xenoliths in older granites and younger granites. Small intrusions and dyke networks of tonalite, granodiorite, granite, ap-lite within the mafic rocks are also characteristic (Fig.2).

These mafic intrusive rocks are generally referred to as "metagabbro-diorite complex" or "epidiorite" (El Ramly and Akaad, 1960; Ghanem, 1972; Dardir and Abu Zeid, 1972; Francis, 1972; Sabet et al., 1972) though they have also been described as gabbro-diorite-tonalite (GDT) by Abdel-Rahman (1990 & 1995). They are a calc-alkaline series believed to have formed in an intra-oceanic subduction zone environment (Abdel-Rahman, 1990), island arc marginal basin (Ghoneim et al., 1992) or active continental margin setting (El-Gharbawi and Hassen, 2001).

Metavolcanic

The exposed Metavolcanics in the study area represent a part of geosynclinal volcanic activity (El Shazly, 1964). According to the latter author, the main geosynclinal volcanics can be distinguished into an older basic series, associated with ultramafics, and a younger series of intermediate composition dominated by andesite together with subordinate diabase and tuffs. Stern (1981) divided the Metavol-

canics cropping out in the area between lat. 25° 30' and 26° 30' N in the Eastern Desert into Older Metavolcanics (OMV) and Younger Metavolcanics (YMV). It covered the vast part of wadi safaga and the mouth of wadis Al Bulah and Abu Furad. The metavolcanics intruded by younger granite (Fig.3).

Tonalites

They covered the wadi Abu Hamur, highly weathered and fractured. It is represented by calc-alkaline foliated (tonalite) rock (Fig.4). This rock is highly fractured and cutted by numerous acidic dikes (felsites and feldspar) (Figs.5&6).

Dokhan Volcanics

It represented by Calc-alkaline andesitic to rhyolitic rocks. They are located at the end of wadi safaga contacted by metagabbro (Fig. 1).

Hammamat Sediments

It located in wadi safaga and extended to south in wadi wasif. The Hammamat metasediments consist mainly of planar bedded and laminated greyish to greenish metasilstone, phyllite and greywacke with minor conglomerate. Graded bedding in the sandstone metasediments indicates consistent upward younging for the sequence (Fig.7).



Fig.4:Tonalite Granite in Wadi Abu Hamur, looking North



Fig.5:Felsite dike intruded in tonalite granite

Younger Granite

This granite restricted in the mouth of wadi safaga. This rock type represented by calc-alkaline, weakly deformed, and deeply weathered (Fig.8). It is intruded in all oldest rocks and intruded by acidic dykes (Fig. 9).

Structure

Faults are essential structural features in the study area (Fig.10). These faults have been well studied in the present work, with emphasis on fault slip. Slickensides and grooves are commonly associated with brittle



Fig.6:Feldspar intruded in tonalite Granite in Wadi Abu Hamur, Looking south



Fig.8:Weathering of Younger Granite in Wadi Safaga, Looking North



Fig.7:Hammamat sediments in Wadi Safaga, Looking South



Fig.9:Acidic Dike intruded in Younger Granite

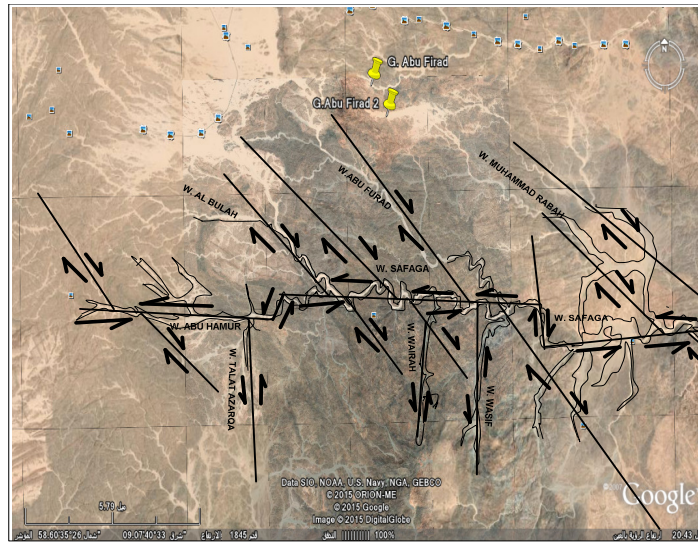


Fig.10: Structure map of the area

faulting. These kinematic indicators indicate the direction and sense of maximum resolved shear stress in that plane (Carey and Brunier, 1974). Slickensides are often composed of fibrous crystals of chlorite, epidote, calcite and quartz that stretch from one side of the fault plane to the other (Fig.11).

The strike-slip faults of NW trends are right-lateral, while those of E-W, NE, and NNE trends are left-lateral faults. These strike-slip faults dislocate the intrusive rocks. Fortunately, the rock exposures provided criteria to evaluate the activity along these faults in chronological order. The NW-trending faults are the oldest fracture planes, followed by the faults of E-W orientation, and ending with the NNE-trending faults (Fig.10). The NNE-trending faults dislocate the older, differently oriented faults. The normal faults are only preserved on a minor scale along these strike-slip faults represented by nearly vertical slickensides that indicate to substantial vertical displacement.

SAMPLING AND TECHNIQUES

A total of 40 stream sedimentary samples were collected from Wadi Abu Hamur-Wadi Safaga through an open bit samples of 50cm diameter and depth of about 80cm., the samples spacing were 750m apart (Fig.1). The average weight of each sample is about 10kg. The obtained samples were dried, sieved using 2mm sieve to remove gravel fraction and the rest of samples were quartered to obtain representative from 120gm up to 200gm from each. The representative samples were prepared for mechanical analysis and mineralogical investigation, where most of the silt and all of the clay were removed by decantation method. A representative sub-sample weighting about 60 gm was taken from each prepared sample and subjected to grain size analysis. The different percentiles were obtained in phi units from the cumulative curves using the phi scale. The four sedimentological statistical parameters namely: the Graphic Mean (M_z), the Inclusive Graphic Standard Deviation (σ_1), the Inclusive Graphic Skewness (Sk), and the Graphic Kurtosis (K_G) were



Fig.11:Slickensides on the fault plane

calculated for each sample, according to the equations quoted by Folk and Ward (1957). The calculated grain size statistical parameters for the sand size fraction are represented in Table (1).

Quantitative mineralogical analyses for the stream sedimentary samples were carried out by gravity separation using a Wilfley Shaking Table (Size No.13), heavy liquid separation using bromoform solution (Sp. Gr. 2.86g/cm³), methylene iodide (Sp. Gr. 3.3g/cm³), and magnetic fractionation using a Frantz Isodynamic Magnetic Separator (Model L-1) to fractionate heavy minerals according to their magnetic susceptibilities. First, magnetite was collected by a hand magnet, and then the magnetite free samples were subjected to the magnetic separation. The condition characterized a Frantz Isodynamic Magnetic Separator transvers slop 5, longitudinal slop 20 and step of current 0.2, 0.5, 1.0, 1.5 magnetic and 1.5 non magnetic current amperes.

Each fraction obtained from the magnetic separation process was microscopically studied under binocular stereomicroscope and investigated to calculate the frequency distribution of the concerned minerals in the studied stream sediment samples.

Mineralogical investigation of the mineral constituents of the stream sediments of Wadi Abu Hamur-Wadi Safaga was carried out by X-ray diffraction technique. A Phillips X-ray diffractometer (Model PW-1010) with a scintillation counter (Model PW-25623/00) and Ni filter was used. Semi-quantitative EDX chemical analyses were carried out using a Phillips XL-30 Environmental Scanning Electron Microscope (ESEM).

Determinations of the eU, eTh, Ra (ppm) and K (%) concentrations of the studied stream sediments were carried out using a Bicon Scintillation Detector NaI (TI) 76x76mm. They were packed in plastic containers, sealed carefully, and stored for thirty days prior to counting.

RESULTS

Grain Size Analyses

The grain size analysis and its distribution is a fundamental descriptive measure for clastic sediments. It is an important parameter in understanding and interpreting the operative mechanism during transportation and for reflecting the sedimentary environments and the processes of sedimentation, as well as, the dynamics affecting of the area.

The four different sedimentological statistical parameters namely: the Graphic Mean (M_z), the Inclusive Graphic Standard Deviation (σ_i), the Inclusive Graphic Skewness (Sk_i), and the Graphic Kurtosis (K_G) were calculated for each sample, according to the equations quoted by Folk and Ward (1957) as follows:

-Graphic Mean (M_z) = $(\phi_{16} + \phi_{50} + \phi_{84})/3$
 -Inclusive Graphic Standard Deviation (σ_i) = $[(\phi_{84} - \phi_{16}) / 4] + [\phi_{95} - \phi_5] / 6.6]$
 -Inclusive Graphic Skewness (Sk_i) = $[(\phi_{16} + \phi_{84} - 2\phi_{50}) / 2(\phi_{84} - \phi_{16})] + [(\phi_5 + \phi_{95} - 2\phi_{50}) / 2(\phi_{95} - \phi_5)]$

-Graphic Kurtosis (K_G) = $(\phi_{95} - \phi_5) / 2.44 (\phi_{75} - \phi_{25})$

The grain size parameters (M_z , σ_i , Sk_i , K_G) were calculated, and the results of these parameters are discussed, and described according to the limits of Folk and Ward (1957), and tabulated in (Table 1) as the follows:

The samples have a graphic mean (M_z) ranging from 0.04 ϕ to 1.8 ϕ (Table 1) which means that it lies in coarse and medium sand size classes represented by 70% and 30% respectively (Table 2).

The samples have inclusive graphic stan-

Table 1: Grain size parameters of the studied samples

Sample	Mean Size (Mz)	Standard Deviation (σ)	Skewness (SKL)	Kurtosis (KG)
1	1.8 Medium sand	1.7 Poorly sorted	0.16 Fine skewed	0.68 Platy kurtic
2	1.4 Medium sand	1.6 Poorly sorted	0.04 Near symmetrical	0.84 Platy kurtic
3	1.3 Medium sand	1.5 Poorly sorted	0.06 Near symmetrical	0.77 Platy kurtic
4	0.95 Coarse sand	1.4 Poorly sorted	0.17 Fine skewed	0.88 Platy kurtic
5	1.6 Medium sand	1.8 Poorly sorted	0.03 Near symmetrical	0.94 Meso kurtic
6	1.1 Medium sand	1.4 Poorly sorted	0.13 Fine skewed	0.86 Platy kurtic
7	0.8 Coarse sand	1.2 Poorly sorted	0.08 Near symmetrical	1.02 Meso kurtic
8	0.3 Coarse sand	1.1 Poorly sorted	0.05 Near symmetrical	0.82 Platy kurtic
9	0.6 Coarse sand	1.2 Poorly sorted	0.03 Near symmetrical	1.26 Lepto kurtic
10	0.3 Coarse sand	0.92 Moderately	0.23 Fine skewed	1.54 Very lepto
11	0.04 Coarse sand	1.1 Poorly sorted	0.15 Fine skewed	1.09 Meso kurtic
12	0.05 Coarse sand	1.1 Poorly sorted	0.26 Fine skewed	1.15 Lepto kurtic
13	0.10 Coarse sand	1.8 Poorly sorted	0.21 Fine skewed	1.13 Lepto kurtic
14	0.18 Coarse sand	1.4 Poorly sorted	0.22 Fine skewed	1.11 Meso kurtic
15	0.19 Coarse sand	0.94 Moderately	0.13 Fine skewed	1.59 Very lepto
16	1.33 Medium sand	1.3 Poorly sorted	0.08 Near symmetrical	0.89 Platy kurtic
17	0.10 Coarse sand	1.3 Poorly sorted	0.33 Strongly fine	1.15 Lepto kurtic
18	0.17 Coarse sand	0.9 Moderately	0.21 Fine skewed	2.05 Very lepto
19	0.15 Coarse sand	0.97 Moderately	0.15 Fine skewed	1.23 Lepto kurtic
20	0.13 Coarse sand	0.88 Moderately	0.09 Near symmetrical	1.04 Meso kurtic
21	1.7 Medium sand	1.72 Poorly sorted	0.17 Fine skewed	0.71 Platy kurtic
22	1.5 Medium sand	1.63 Poorly sorted	0.05 Near symmetrical	0.82 Platy kurtic
23	1.4 Medium sand	1.51 Poorly sorted	0.05 Near symmetrical	0.75 Platy kurtic
24	0.9 Coarse sand	1.42 Poorly sorted	0.18 Fine skewed	0.89 Platy kurtic
25	1.61 Medium sand	1.7 Poorly sorted	0.05 Near symmetrical	0.96 Meso kurtic
26	1.12 Medium sand	1.5 Poorly sorted	0.13 Fine skewed	0.88 Platy kurtic
27	0.9 Coarse sand	1.2 Poorly sorted	0.09 Near symmetrical	1.03 Meso kurtic
28	0.31 Coarse sand	1.2 Poorly sorted	0.04 Near symmetrical	0.84 Platy kurtic
29	0.62 Coarse sand	1.4 Poorly sorted	0.03 Near symmetrical	1.27 Lepto kurtic
30	0.31 Coarse sand	0.95 Moderately	0.24 Fine skewed	1.6 Very lepto
31	0.06 Coarse sand	1.14 Poorly sorted	0.16 Fine skewed	1.1 Meso kurtic
32	0.05 Coarse sand	1.13 Poorly sorted	0.28 Fine skewed	1.14 Lepto kurtic
33	0.11 Coarse sand	1.81 Poorly sorted	0.23 Fine skewed	1.15 Lepto kurtic
34	0.17 Coarse sand	1.5 Poorly sorted	0.24 Fine skewed	1.12 Meso kurtic
35	0.19 Coarse sand	0.96 Moderately	0.15 Fine skewed	1.57 Very lepto
36	1.4 Medium sand	1.35 Poorly sorted	0.09 Near symmetrical	0.99 Platy kurtic
37	0.12 Coarse sand	1.4 Poorly sorted	0.34 Strongly fine	1.16 Lepto kurtic
38	0.19 Coarse sand	0.92 Moderately	0.22 Fine skewed	2.1 Very lepto
39	0.14 Coarse sand	0.87 Moderately	0.15 Fine skewed	1.21 Lepto kurtic
40	0.13 Coarse sand	0.89 Moderately	0.09 Near symmetrical	1.05 Meso kurtic

standard deviation (σ_s) ranging from 0.88 to 1.8 (Table 1), the samples could be categorized in the poorly sorted class and moderately sorted represented by 75% and 25%, respectively (Table 2).

The samples have inclusive graphic Skewness (Sk_g) ranging from 0.03 to 0.33 (Table 1), the samples could be categorized in fine skewed, near symmetrical, and strongly fine skewed classes represented by 55%, 40%, and 5%, respectively (Table 2).

The samples have inclusive graphic Kurtosis (K_g) ranging from 0.68 to 2.05 (Table 1), the samples could be categorized in the platykurtic, mesokurtic and very leptokurtic classes represented by 35%, 25%, 15% and 25%, respectively (Table 2).

Shape and size are quite important for measuring of the textural maturity of the sediment and the texture as a key of the sedimentary deposit history. So the sorting is reflected the sedimentary history of the deposit. It shows the nature and magnitude of the weathering (transportation, and deposition processes and their duration). The sediments are characterized by poorly to moderately sorted sediment texture and medium to coarse grain size that reflect their immature texture.

The skewness is a measure of the symmetry of the frequency curve. The frequency curve is represented by bimodal. The bimodal curve may be due to the following:

a) Effect of source rock: by mechanical weathering of rocks such as granite where two major size are present (medium and coarse), the resulting sediments will have two large amounts related to the two different major sizes (bimodal).

b) Turbulent transportation: Turbidity currents can cause the admixing of sediments from different environments. Turbulent flow is a motion in which velocity fluctuates and direction changes during flow. The material carried is usually of mixed nature and accordingly of less sorted type. The turbulent flow is the ability to carry coarse-grained materials.

EVALUATION OF THE STREAM SEDIMENTS

Heavy Minerals Distribution

To obtain the heavy minerals from the studied stream sediment samples gangue minerals should be removed, especially quartz and feldspars which constitute more than 90% of the stream sediments of Wadi Abu Hamur-Safaga by using the shaking table, then path through the heavy liquid as bromoform and methylene.

The percent of the heavy minerals content in the studied stream sediments are tabulated in Table 3. The heavy minerals content ranging from 2% and 10.5% with an average of 4.5% (Fig.12).

Table 2: Distribution of the different calculated grain size parameters of the studied samples among the different classes

Graphic Mean M_z		Inclusive Graphic		The Inclusive Graphic		The Inclusive Kurtosis	
Class	%	Class	%	Class	%	Class	%
Coarse	70	Poorly sorted	75	Fine skewed	5	Platykurtic	35
Medium	30	Moderately sorted	25	Near symmetrical	4	Mesokurtic	25
				Strongly fine skewed	5	Very leptokurtic	15
						Leptokurtic	25

The high content of the heavy minerals in the studied stream sediments restricted in some localities near the acidic rocks.

The obtained fractions were weighted and their percentages were calculated (Table 4). It

is obviously noted that the heavy minerals are concentrated mainly in 0.2 amp and 0.5 amp magnetic fractions; while 1.5amp magnetic and non-magnetic fractions contains the lowest concentration of the heavy minerals.

A considerable number of grains from each magnetic fraction were counted (about 1500 grains). The weight percentage of each concerned mineral relative to the corresponding original sample was calculated according to Stakhove equation:

$$Q = [P \cdot n_m \cdot d_m / \Sigma(n_o d_o)].100$$

Where: Q = the weight percentages of the concerned mineral

P = the weight percentage of the corresponding magnetic fraction.

n_m = the number of grains of the mineral.

d_m = specific gravity of the mineral.

$\Sigma(n_o d_o)$ = the sum of the number of grains for each mineral multiplied by its specific gravity.

The common heavy minerals in the studied stream sediments are zircon, titanite, monazite, garnet, rutile, fluorite, thorite, green silicates (amphipoles & pyroxenes) in addition to opaque minerals magnetite, ilmenite and hematite (Tables 5 a & b).

Iron Oxides Minerals

Magnetite

It represents the major part of opaque grains of the studied samples. It is black granular masses (Fig.13), and strongly magnetic, sometimes with zircon or garnet inclusions. It separated using small hand magnet. These mineral constituents range from 0.1% to 2.3 % with an average 1.07 %, and are represented by histogram (Fig.14).

The low uranium and thorium contents in magnetite of the stream sediments indicate that uranium in magnetite is mostly of the adsorbed type which is liable and easily leachable under the weathering conditions

Table 3: The percentages of the heavy minerals in the studied stream sediments of Wadi Abu Hamur-Safaga after Bromoform

Name of Wadi	S. No.	Heavy Min. %	Name of Wadi	S. No.	Heavy Min. %
Abu Hamur	1	5.01	Safaga	21	3.17
	2	7.21		22	3.041
	3	5.71		23	3.841
	4	7.03		24	4.11
	5	6.74		25	3.91
	6	7.12	Abu Furad	26	4.01
	7	6.44	Safaga	27	2.96
	8	9.62		28	3.14
	9	4.83		29	4.03
	10	4.22		30	4.38
	11	5.1		31	4.07
El Bula	12	5.3	32	3.93	
Safaga	13	6.22	33	4.78	
	14	6.19	34	1.77	
	15	4.66	35	2.632	
	16	3.93	36	3.152	
	17	3.75	37	3.982	
	18	4.13	38	4.322	
	19	2.57	39	4.712	
	20	2.29	40	5.112	
	Min.				1.77
Max.				9.62	
Ave.				4.58	

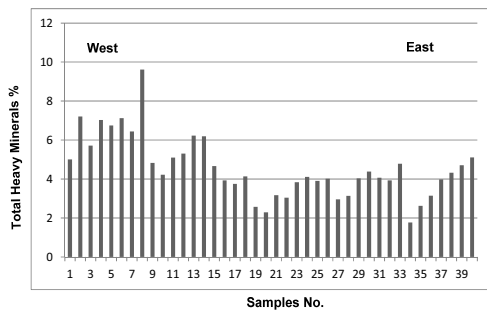


Fig.12:Histogram show the distribution of total heavy minerals in the study area

Table 4: Frequency of the heavy minerals in the different magnetic fractions

S. No.	Magn. %	0.2 mag. %	0.5 mag. %	1.0 mag. %	1.5 mag. %	1.5 Non mag. %
S1	15.6	33.8	43.6	3.20	0.72	2.031
S2	35.95	24.6	36.7	1.33	0.11	1.296
S3	13.2	58.7	23.5	2.38	0.77	1.460
S4	30.8	42.1	21.5	4.00	1.14	9.507
S5	14.2	40.3	40.3	2.35	0.22	2.593
S6	25.3	39.7	26.5	1.93	1.04	5.510
S7	18.0	36.9	37.7	2.87	0.30	4.309
S8	28.7	33.8	35.2	0.59	0.22	1.476
S9	14.2	18.3	25.2	0.55	0.10	0.305
S10	12.4	14.3	16.6	0.97	0.13	0.507
S11	13.5	41.9	16.6	0.58	0.10	0.642
S12	12.8	42.1	20.1	0.52	0.25	0.642
S13	14.7	39.1	21.2	0.31	0.26	0.63
S14	15.4	38.5	18.5	0.13	0.19	0.55
S15	17.2	35.6	17.5	0.78	0.19	0.64
S16	18.3	30.7	19.7	0.33	0.14	0.75
S17	14.5	32.1	20.2	0.21	0.52	0.81
S18	17.5	40.5	25.5	0.25	0.34	0.94
S19	15.0	36.2	28.6	0.17	0.62	0.92
S20	13.0	30.5	30.1	0.91	0.75	0.95
S21	11.0	28.9	30.5	0.52	0.53	0.98
S22	12.0	28.6	22.2	0.13	0.62	0.88
S23	16.0	25.7	25.6	0.21	0.28	0.71
S24	15.0	35.7	33.3	0.17	0.31	0.60
S25	20.0	35.8	31.5	0.19	0.42	0.58
S26	21.0	36.3	29.8	0.95	0.20	0.52
S27	20.1	30.1	28.2	0.21	0.36	0.62
S28	19.0	29.5	25.1	0.19	0.41	0.51
S29	18.0	28.6	25.1	0.17	0.24	0.53
S30	16.21	27.5	20.1	0.17	0.21	0.32
S31	15.32	32.0	18.5	0.15	0.31	0.41
S32	13.02	31.2	15.4	0.14	0.34	1.1
S33	14.21	26.5	17.3	0.13	0.26	1.2
S34	16.1	27.4	22.1	0.18	0.5	0.54
S35	17.2	29.3	21.5	0.19	0.8	0.62
S36	18.4	30.1	23.6	1.1	1.1	1.4
S37	19.45	37.2	21.4	1.7	1.3	1.2
S38	16.1	34.13	28.5	2.43	2.15	1.83
S39	19.4	36.78	26.8	2.97	1.13	1.57
S40	20.54	36.87	26.6	2.58	1.40	1.60
Min.	11	24.6	15.4	0.13	0.1	0.305
Max.	35.95	58.7	43.6	4	2.15	9.507
Aver.	23.5	40.8	29.6	2.1	1.1	4.8

by meteoric water.

Hematite

Hematite has a wide range of distribution as magnetite and both are present in the first two fractions in the stream sediments samples. It is considered as the major heavy mineral in the host rock samples (Fig.15). These mineral constituents range from 0.01% to 0.4% with an average of 0.1 %, and represented by histogram (Fig.16). The Semi quantitative analy-

ses (EDX) show high iron content with low content of Titanium, Manganese (Fig.17).

Ilmenite [FeTiO₃]

The ilmenite grains of the stream sediments may be altered. It concentrated in a relatively the highly magnetic fraction at 0.2 amp. It is the most abundant Fe-Ti oxide mineral that occurs in a wide variety of igneous rocks, some metamorphic rocks, and as detritus mineral grains. Ilmenite in the studied stream sedi-

Table 5a: The weight percentages of the concerned heavy minerals in the studied stream sediment samples.

S. No.	Gar. %	Rut. %	Tit. %	Flu. %	Zr. %	Mz. %	Tho. %	Amph. & Pyr. %
1	0.1	0.3	0.2	0.01	0.1	0.05	0.01	2.04
2	0.3	0.5	0.1	0.01	0.3	0.07	0.02	3.11
3	0.2	0.6	0.3	0.01	0.5	0.03	0.01	1.96
4	0.4	0.8	0.4	0.03	0.6	0.06	0.03	1.51
5	0.2	0.5	0.3	0.03	0.4	0.01	0.01	3.69
6	0.3	0.7	0.2	0.02	0.6	0.01	0.01	3.78
7	0.1	0.9	0.3	0.04	0.7	0.02	0.02	2.56
8	0.2	1.1	0.5	0.02	0.9	0.04	0.03	3.63
9	0.06	0.3	0.4	0.03	0.1	0.01	0.001	2.33
10	0.1	0.2	0.3	0.01	0.2	0.01	0.001	1.9
11	0.3	0.4	0.2	0	0.5	0.04	0.03	1.73
12	0.1	0.2	0.1	0	0.3	0.001	0.001	2.2
13	0.3	0.3	0.22	0	0.4	0.001	0	3.1
14	0.04	0.25	0.2	0	0.2	0.01	0	3.1
15	0.03	0.4	0.1	0	0.1	0	0	2.9
16	0.01	0.2	0.02	0	0.08	0	0	2.7
17	0.02	0.21	0.03	0	0.08	0	0	2.5
18	0.02	0.18	0.01	0	0.05	0.001	0	2.8
19	0.01	0.15	0.01	0	0.05	0.001	0	1.5
20	0.01	0.12	0.01	0	0.04	0.001	0	1.4
21	0.01	0.10	0.01	0	0.03	0.001	0	2.1
22	0.03	0.2	0.01	0	0.02	0.001	0	2.2
23	0.04	0.22	0.02	0	0.05	0.001	0	3.1
24	0.04	0.3	0.03	0	0.07	0	0	3.2
25	0.03	0.2	0.02	0	0.02	0	0	3.4
26	0.01	0.1	0.02	0	0.01	0	0	3.5
27	0.05	0.1	0.1	0	0.2	0	0	2.2
28	0.04	0.21	0.1	0	0.06	0	0	2.3
29	0.05	0.1	0.1	0	0.04	0	0	2.8
30	0.02	0.2	0.1	0	0.06	0	0	3.0
31	0.01	0.1	0.2	0	0.04	0	0	3.1
32	0.01	0.1	0.1	0	0.03	0	0	3.2
33	0.04	0.2	0.3	0	0.02	0	0	3.5
34	0.07	0.18	0.3	0	0.01	0	0	0.1
35	0.1	0.3	0.5	0.1	0.05	0.001	0.001	0.1
36	0.2	0.4	0.6	0.02	0.07	0.001	0.001	0.1
37	0.4	0.5	0.6	0.02	0.06	0.001	0.001	0.1
38	0.3	0.5	0.7	0.02	0.1	0.001	0.001	0.1
39	0.5	0.6	0.7	0.01	0.1	0.001	0.001	0.1
40	0.5	0.6	0.7	0.01	0.1	0.001	0.001	0.1
Min.	0.01	0.1	0.01	0.01	0.01	0.001	0.001	0.1
Max.	0.5	1.1	0.7	0.03	0.9	0.07	0.03	3.78
Aver.	0.131	0.19	0.228	0.008	0.18	0.001	0.001	2.2185

Gar.=garnet, Rut.=rutile, Flu.= Fluorite, Tit.=titanite, Zr.=zircon, Mz.=monazite, Thrt.=thorite, Amph.&Pyr.=amphiboles and pyroxenes.

Table 5b: The weight percentages of the concerned heavy minerals in the studied stream sediment samples

S. No.	Mag.	Ilm.	Hm.
1	1.5	0.5	0.2
2	1.8	0.8	0.2
3	1.4	0.6	0.1
4	2	0.9	0.3
5	1.2	0.3	0.1
6	1.1	0.2	0.2
7	1.3	0.3	0.2
8	2	0.9	0.3
9	1.3	0.2	0.1
10	1.1	0.3	0.1
11	1.6	0.1	0.2
12	1.7	0.4	0.3
13	1.0	0.5	0.4
14	2.1	0.2	0.1
15	1	0.1	0.03
16	0.8	0.1	0.02
17	0.7	0.2	0.01
18	0.9	0.14	0.03
19	0.7	0.12	0.03
20	0.6	0.1	0.01
21	0.8	0.1	0.02
22	0.4	0.15	0.03
23	0.2	0.2	0.01
24	0.15	0.3	0.02
25	0.1	0.13	0.01
26	0.2	0.14	0.03
27	0.1	0.2	0.01
28	0.2	0.21	0.02
29	0.4	0.5	0.04
30	0.8	0.1	0.1
31	0.5	0.1	0.02
32	0.4	0.08	0.01
33	0.5	0.2	0.02
34	1	0.07	0.04
35	1.2	0.3	0.07
36	1.5	0.2	0.06
37	1.9	0.3	0.1
38	2.2	0.3	0.1
39	2.1	0.4	0.2
40	2.3	0.5	0.3
Min.	0.1	0.07	0.01
Max.	2.3	0.9	0.4
Aver.	1.069	0.29	0.104

Mag.=magnetite, Ilm.=ilmenite, Hm.=hematite

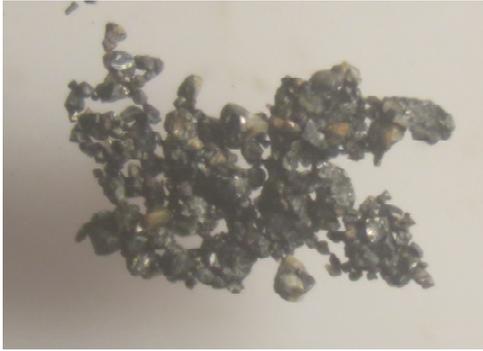


Fig.13:Photomicrograph of magnetite

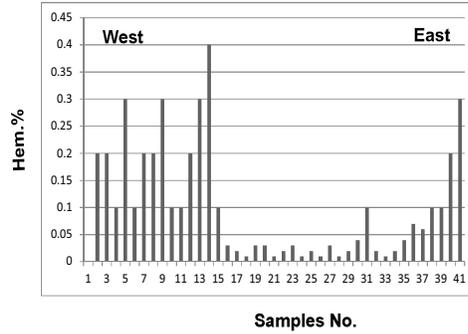


Fig.16:Histogram distribution of hematite

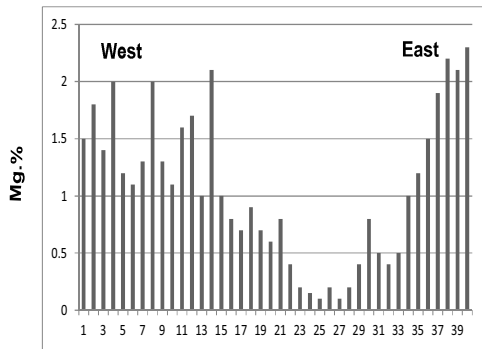


Fig.14:Histogram distribution of magnetite

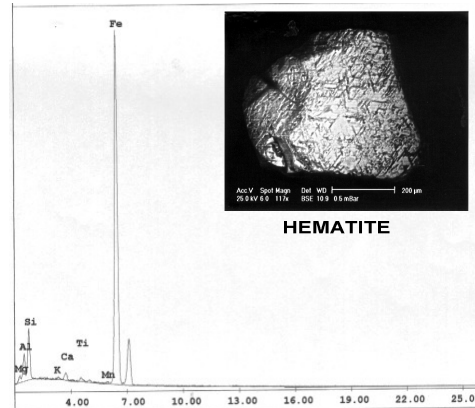


Fig.17: (EDX) ESEM hematite analysis



Fig.15:Photomicrograph of hematite

ments occurs as irregular, tabular or massive to subrounded, angular grains (Fig. 18). These grains exhibit black to brownish black colors and submetallic to metallic luster. The brownish tint of some ilmenite grains may be due to the partial alteration of these grains. These mineral constituents range from 0.07% to 0.9 % with an average of 0.29%, and represented by histogram (Fig.19).

Garnet

The minerals of garnet group characterize some metamorphic rocks and in some igneous rock types, and can be noticed generally as detritus grains in sediments. It exhibits dif-

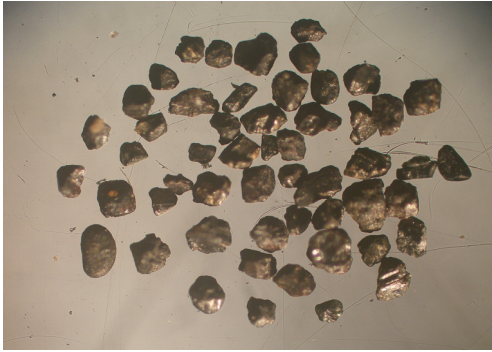


Fig.18:Photomicrograph of ilmenite

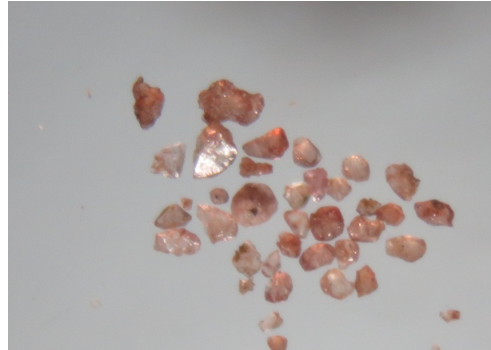


Fig.20:Photomicrograph of garnet

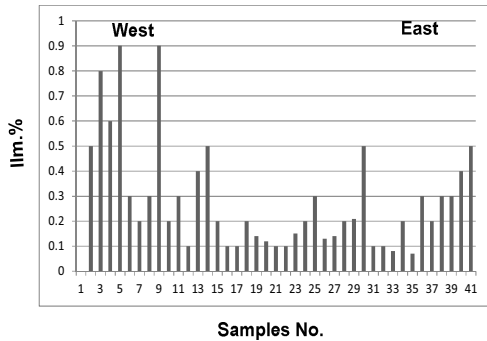


Fig.19 Histogram distribution of ilmenite

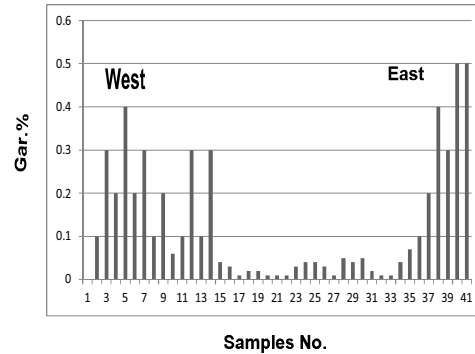


Fig.21:Histogram distribution of garnet

ferent colors ranging from pale pink to dark brown with vitreous luster. Sometimes, garnet grains appear to be cloudy due to staining or inclusions (Fig.20). The almandine type is the common garnet mineral in the studied samples, probably due to the effect of contact or regional metamorphism. These mineral constituents range from 0.01% to 0.5% with an average of 0.13%, and represented by histogram (Fig.21). The garnet in the studied stream sediments was confirmed either by ESEM (Fig.22).

TITANIUM MINERALS

Rutile [TiO₂]

It is the preferred mineral for the production of titanium dioxide. Rutile mineral grains

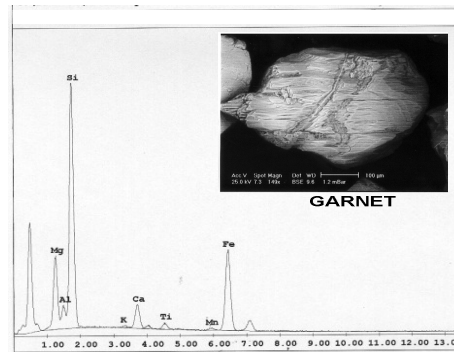


Fig.22: ESEM garnet analysis

are commonly prismatic, elongated, tabular and massive granular in shape. The common colors of rutile are reddish brown grading into the red (Fig.23) and black with adamantine luster. These mineral constituents ranged from 0.1% to 1.1% with an average of 0.188%, and represented by histogram (Fig.24).

Titanite (Sphene) [CaTiSiO₅]

It is widespread in acidic and intermediate igneous rocks, and in several metamorphic rocks as accessory phase. It exhibits transparent to translucent yellow to yellowish brown colours (Fig.25). Titanite mineral grains are subhedral to anhedral grains of adamantine luster and imperfect cleavage. The presence of titanite in the studied sediments was confirmed either by ESEM (Fig.26), and X-ray diffraction (Table 6). These mineral constituents ranged from 0.01% to 0.7% with an average of 0.23%, and represented by the histogram (Fig.27).

Fluorites

Fluorite is present in the stream sediments as coarse grains. It is whitish or pale yellow in color and has irregular wedge shape (Fig.28). Fluorite may have been originated from the granitic magma during the differentiation, or later at the deuteric stage forming the coarser fluorite sizes. These mineral con-

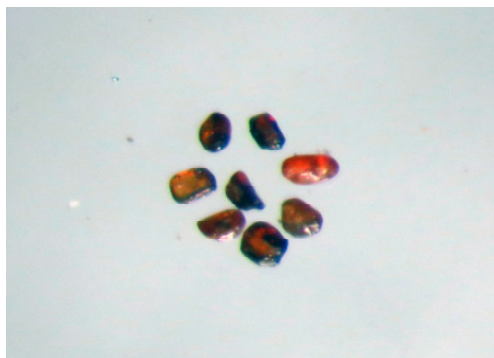


Fig.23:Photomicrograph of rutile

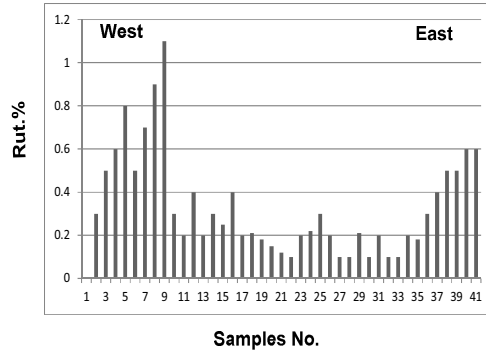


Fig.24:Histogram distribution of rutile

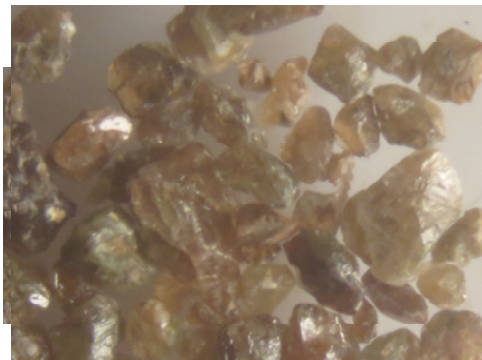


Fig.25:Photomicrograph of titanite

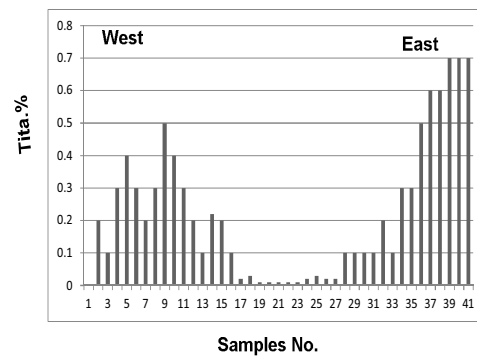


Fig.26:Histogram distribution for titanite

Table 6: X-ray diffraction data of titanite of Wadi Abu Hamur-Safaga area

Analysed Sample		Titanite ASTM card (11-446)	
dA	I/I ₀	dA	I/I ₀
7.22	6		
4.95	23	4.93	30
3.24	100	3.233	100
3.00	97	2.989	90
2.61	67		
2.59	55	2.595	90
2.29	19	2.273	30
2.07	27	2.058	40
1.65	24	1.643	40
1.50	17	1.494	4

stituents ranged from 0.01% to 0.03% with an average of 0.0075%, and represented by the histogram (Fig.29).

RADIOACTIVE MINERALS

Zircon [ZrSiO₄]

Zircon is a remarkable mineral due to its ubiquitous occurrence in crustal igneous, metamorphic and sedimentary rocks, and in even mantle xenoliths, lunar rocks, meteorites and tektite (Speer, 1980). It occurs as an euhedral to subhedral grains, Prismatic with bi-pyramidal termination (Fig.30a), and two bi-pyramidal (Fig.30b). It is exhibiting brownish yellow colours of adamantine luster. These mineral constituents range from 0.01% to 0.9% with an average 0.184%, and represented by histogram (Fig.31). ESEM data (EDX) indicate that zircon consists mainly of ZrO₂ and SiO₂ with trace amounts of Ca, Hf, Fe and Al (Fig.32). The Zr/Hf ratio is a principle indicator of magmatic differentiation. The average Zr/Hf of zircon from granitoid rocks is 37.3, while this ratio reaches to 49.6 for volcanic rocks, 55.7 for basic rocks and 67 for ultrabasic rocks (Lyakhvich and Vishnevskiy, 1990). For the studied zircon, Zr/Hf ranges from 31.15 to 41.78, indicating that they derived from granitoid rocks.

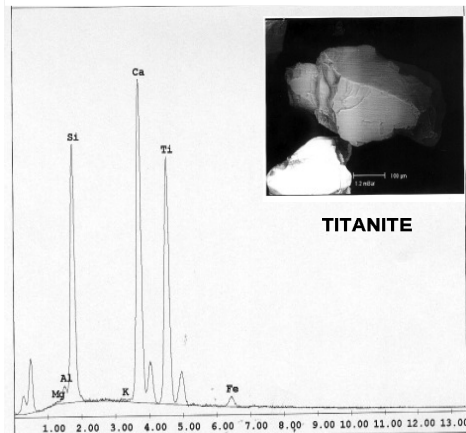


Fig.27: ESEM titanite analysis



Fig.28: Photomicrograph of fluorite

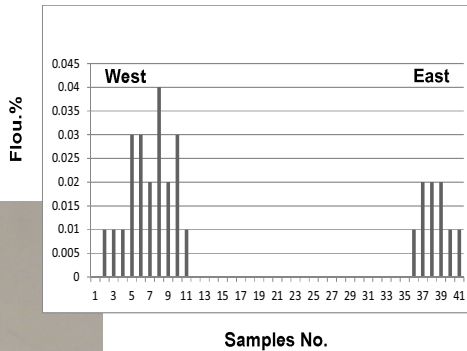


Fig.29: Histogram distribution of fluorite

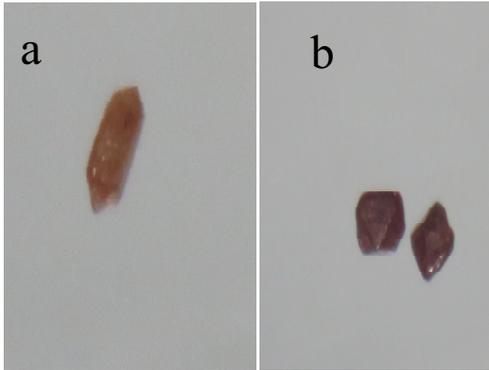


Fig.30 a&b: Photomicrograph of zircon

Monazite [CeLaPO₄]

It is one of the most important nuclear minerals, being a major host for REEs and actinides Th and U (Hinton and Paterson 1994, Bea et al., 1994 and Bea 1996). Monazite in the studied samples is rare in the heavy minerals of these samples. It forms tabular and broken crystals. Most of these grains are characterized by pitted surfaces. It is pale yellow, honey yellow, greenish yellow and reddish yellow colour grains. These mineral constituents ranged from 0.001% to 0.07% with an average of 0.001% and represented by the histogram (Fig.33). The EDX data (Fig.34).

Thorite [ThSiO₄]

It occurs widely in the form of accessory minerals, which belong to the most important basic commercial minerals of thorium. It occurs as brownish black to black opaque grains of greasy luster (Fig.35). Most of thorite mineral grains are subhedral to anhedral corroded and cracked. These mineral constituents range from 0.001% to 0.03% with an average 0.001 %, and represented by histogram (Fig. 36).

They are strongly metamictized, as determined by X-ray diffraction. In nature, thorite, generally, occurs in metamict state, amorphous to X-ray and electron diffraction, even though,

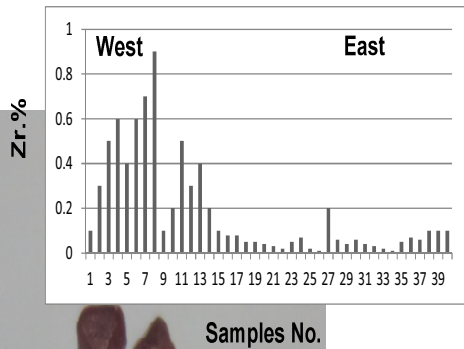


Fig.31:Histogram distribution for zircon

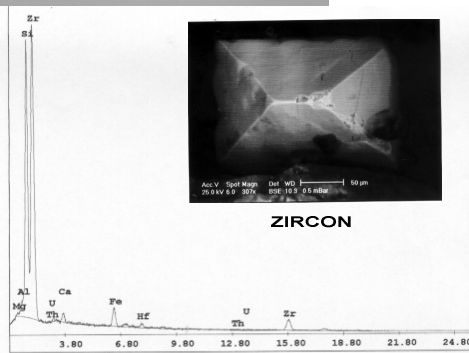


Fig.32:ESEM zircon analysis

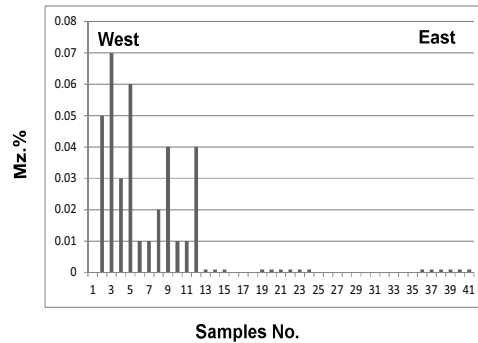


Fig.33: Histogram distribution of monazite

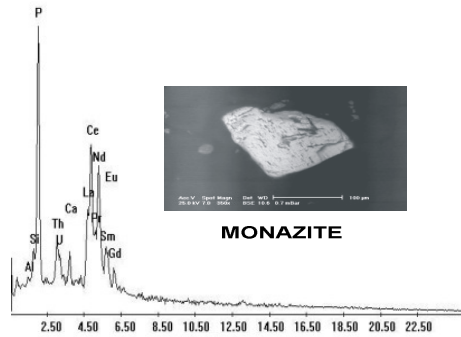


Fig.34:(EDX) ESEM monazite



Fig.35:Photomicrograph of thorite

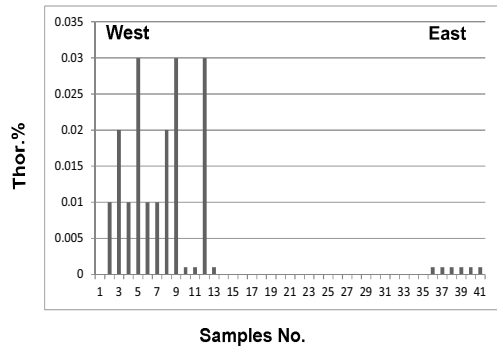


Fig.36:Histogram distribution of thorite

they may have crystal faces (Palache et al. 1944, Pabst 1952, Ewing and Haaker 1980). Thorite was annealed at 1100°C for approximately four hours preceding identification by XRD. The obtained data (Table 7) reveal the presence of thorite peaks (ASTM card 11-419) in addition to hematite peaks (ASTM card 13-534). The presence of hematite may be in the form of thin films coating thorite grains or as individual hematite grains. The ESEM analysis shows that thorite consists mainly of ThO₂ and SiO₂. Minor and trace elements include Y, U, Ca, Fe and REE (Fig. 37).

Amphiboles and Pyroxenes

These minerals consists of amphiboles, pyroxene, biotite, muscovite and epidote, and detected in the stream sediments. These minerals may have originated from igneous rocks. These minerals are characterized by coarse size detrital particles, black, green to pale green colour (Fig.38) and has medium to high magnetic success-ability. These mineral constituents range from 0.1% to 3.78% with an average of 2.22 %, and represented by histogram (Fig.39).

RADIOMETRIC STUDY

The collected samples has been subjected to radiometric analyses to the studied area determine variations in eU, eTh, Ra and K%. The obtained results from the radiometric measurements of the studied stream sediments are listed in Table 8, and calculate the ratios of eU/eTh and eU/Ra. Draw the histograms distribution for these elements and ratios (Figs. 40 & 41).

The examined stream sediments of Wadi Abu Hamur-Safaga are characterized by radiometrically (low to moderately) concentrations of eU and eTh. The radiometrically elemental concentration of eU range between 1 and 4ppm with an average of 1.76ppm, while eTh is between 2 and 29ppm with an average of 10.75 ppm. The average Ra content for these sediments is 2.89ppm, ranging between

Table 7: X-ray diffraction data of the annealed thorite from the studied stream sediments

Analyzed Sample		Thorite		Hematite	
dÅ	I/I ₀	dÅ	I/I ₀	dÅ	I/I ₀
4.67	59	4.72	85		
3.54	100	3.55	100	3.66	25
2.82	21	2.842	45		
2.70	32			2.69	100
2.64	46	2.676	75		
2.52	21	2.516	30	2.51	50
2.34	3	2.361	5		
2.20	22	2.222	30	2.201	30
2.07	2			2.07	2
1.99	9	2.019	20		
1.87	15	1.885	30		
1.82	28	1.834	65	1.838	40
1.77	10	1.782	20		
1.69	12			1.69	60
1.65	8	1.667	10	1.634	4
1.48	5	1.484	20	1.484	35
1.43	4	1.444	15	1.453	35

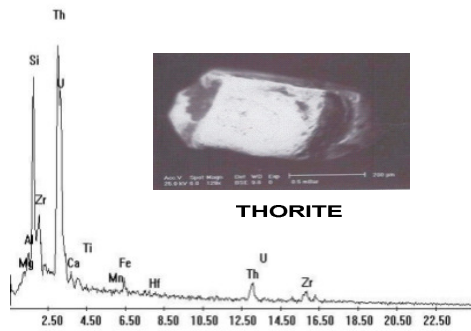


Fig.37: (EDX) ESEM thorite

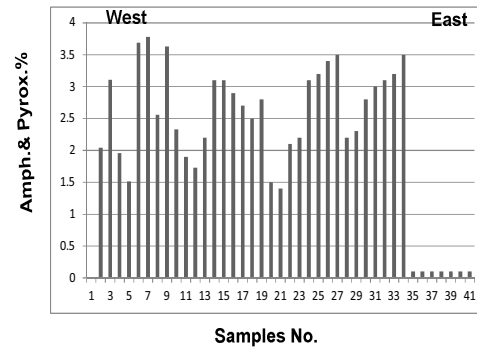


Fig.39: Histogram distribution of amphiboles and pyroxenes

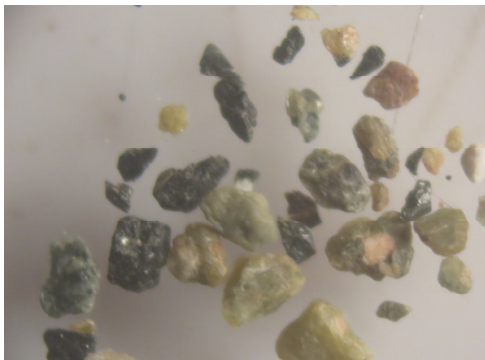


Fig.38: Photomicrograph of amphiboles and pyroxenes

1 and 5ppm. The average content of K% 1.16%, ranging between 0.1 and 1.56.

Ivanovich (1994) concluded that a relatively constant Th/U mass ratio of around 3.5 is found in most natural systems. The average of the corresponding value (eTh/eU ratio) for the sediments of Wadi Abu Hamur-Safaga is 5.48 varying between 1.33 and 12.5 which indicate that there is a significant fractionation during weathering of these sediments causing the depletion of U.

Table 8: eU, eTh, Ra (ppm) and K (%) content of the Wadi Abu Hamur-Safaga stream sediments

S. No	eU (ppm)	eTh (ppm)	Ra (ppm)	K (%)	eTh/eU	ARs (eU/Ra)
S1	2	10	1	1.48	5	2
S2	1	18	2	1.56	18	0
S3	3	20	3	1.12	6.7	1
S4	4	16	2	1.05	4	2
S5	4	17	3	1.07	4.25	1
S6	2	24	4	1.01	12	0
S7	3	28	4	1.18	9.33	0
S8	4	23	4	0.92	5.75	1
S9	2	10	3	1.04	5	0
S10	1	9	3	1.27	9	0
S11	1	8	2	0.92	8	0
S12	1	7	1	1.48	7	1
S13	1	6	2	1.56	6	0
S14	1	7	3	1.12	7	0
S15	1	5	2	1.05	5	0
S16	1	4	3	1.07	4	0
S17	1	6	4	1.01	6	0
S18	1	3	4	1.18	3	0
S19	1	5	4	0.92	5	0
S20	1	4	3	1.04	4	0
S21	1	3	3	1.27	3	0
S22	1	2	2	0.92	2	0
S23	1	2	2	0.1	2	0
S24	1	2	1	1.48	2	1
S25	1	2	2	1.56	2	0
S26	1	3	3	1.12	3	0
S27	1	3	2	1.05	3	0
S28	1	4	3	1.07	4	0
S29	1.5	5	4	1.01	1.33	0
S30	1	6	4	1.18	6	0
S31	2	5	4	0.92	2.5	0
S32	2	7	3	1.04	3.5	0
S33	3	8	3	1.27	2.7	1
S34	2	15	2	0.92	7.5	1
S35	2	18	3	1.1	9	0
S36	2	16	4	1.5	8	0
S37	3	21	5	1.4	7	0
S38	3	24	3	1.3	8	1
S39	2	25	5	1.5	12.5	0
S40	3	29	4	1.5	9.7	0
Aver.	1.76	10.75	2.98	1.16	5.48	0
Min.	1	2	1	0.1	1.33	0
Max.	4	29	5	1.56	12.5	2

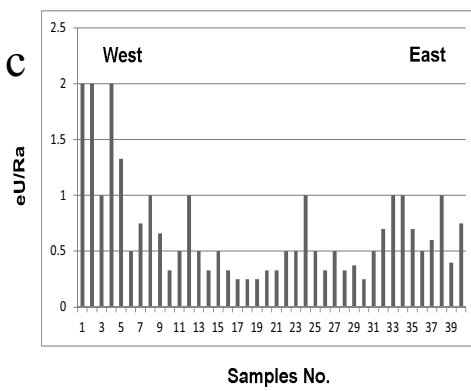
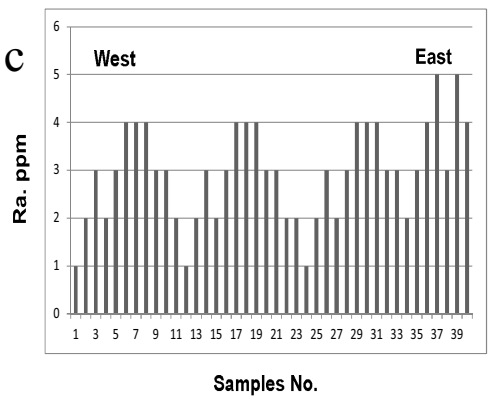
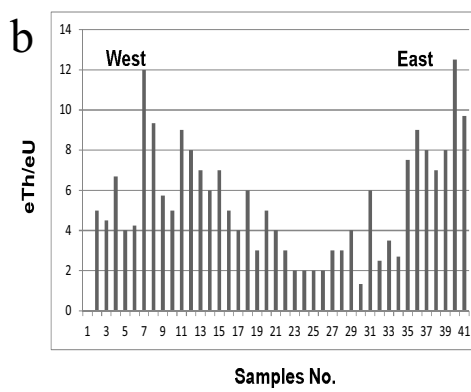
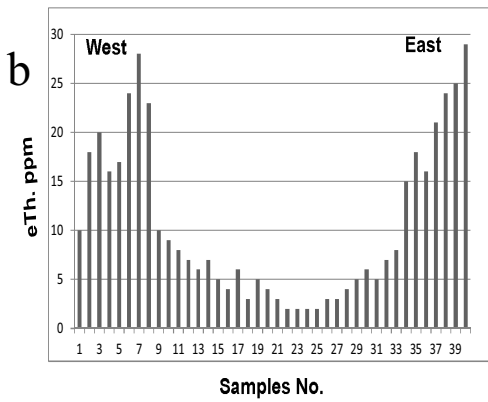
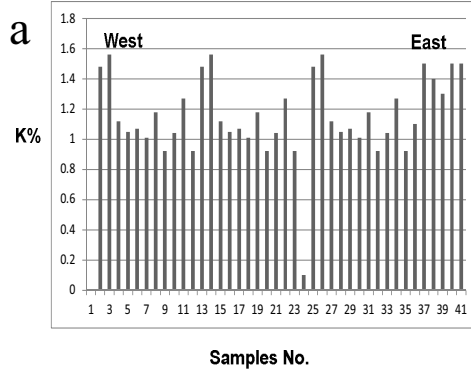
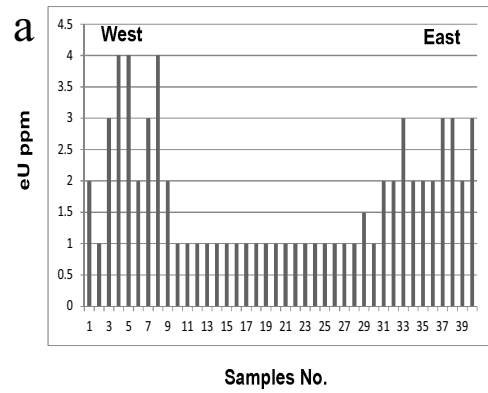


Fig.40 a,b&c:Histograms distribution of equivalent uranium, thorium, and Ra ppm

Fig.41_a,b&c: Histograms distribution of K%, eTh/eU, and eU/Ra

The main factors controlling the distribution of radioelements in sediments are the geomorphological features of the basin of deposition, radioelements content of the source rocks, grain size of these sediments, the alkalinity of the surface groundwater, and to a lesser extent effect of the organic matter. $^{238}\text{U}/^{226}\text{Ra}$ activity ratios (ARs) can be used to ascertain equilibrium within the same decay series (Navas et al., 2002). If secular equilibrium prevails in the ^{238}U chain, ARs of $^{238}\text{U}/^{226}\text{U}$ will be approximately 1, ARs values other than 1 indicate disequilibrium. The ARs for the studied stream sediments of Wadi Abu Hamur-Safaga alternate lower and higher than 1, which indicate a state of disequilibrium in these sediments.

eU Versus eTh Variation Diagram

The relation between U and Th may indicate the enrichment or depletion of U because Th is chemically stable. The eU against eTh variation diagram for the studied samples is shown on Figure 42, which indicates strong positive relationships between the two elements. This result explains the low alteration processes affecting these samples, and also indicates that magmatic processes played an important role in the uranium enrichment of these granites which represent the source of these sediments.

eU Versus Zr Variation Diagram

The eU versus Zr variation diagram shows strong positive correlation in the studied samples (Fig.43). The uranium and zirconium enrichment in the studied samples, supports the concept that U was trapped in the accessory minerals as zircon and the uranium is magnetically.

CONCLUSIONS

This study of economic minerals in the stream sediments of wadi Abu Hamur-wadi Safaga which has long 30km and width reach to 50m. The area covered by igneous and met-

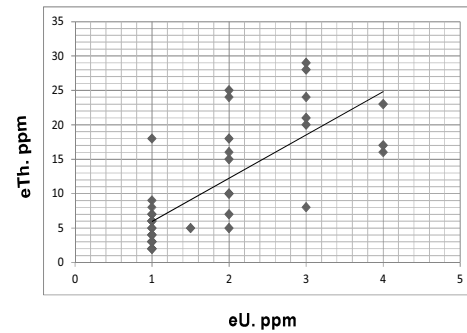


Fig.42:Direct relationship between equivalent uranium and equivalent thorium

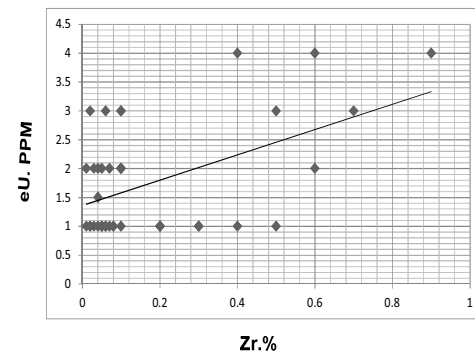


Fig.43:Direct relationship between eU and concentration of Zr minerals

amorphic rocks represented by Metagabbro, Metavolcanic, Older Granite, Dokhan Volcanics, Hammamat Sediments and Younger Granite.

The area affected by different faults and represented by strike-slip faults of NW trends are right-lateral, while those of E-W, NE, and NNE trends are left-lateral faults. The normal faults are only preserved on a minor scale along these strike-slip faults represented by nearly vertical slickensides that indicate to substantial vertical displacement.

The grain size analysis and its distribu-

tion is a fundamental descriptive measure for clastic sediments. The results of statistical parameters a graphic mean (M_z) lies in coarse and medium sand size classes represented by 70% and 30%, respectively, inclusive graphic standard deviation (σ_i) could be categorized in the poorly sorted class and moderately sorted represented by 75% and 25% respectively, inclusive graphic Skewness (Sk_i) could be categorized in fine skewed, near symmetrical, and strongly fine skewed classes represented by 55%, 40%, and 5%, respectively, and inclusive graphic Kurtosis (K_g) could be categorized in the platykurtic, mesokurtic, very leptokurtic and leptokurtic classes represented by 35%, 25%, 15% and 25%, respectively.

The average content of total heavy minerals is 4.5% and the heavy content ranging from 2% and 10.5%. Opaque minerals represented by Magnetite, Hematite, Ilmenite constituents have an average 1.07 %, 0.1 % and 0.286% respectively. Abrasive minerals as Garnet constituents has an average 0.13% and pigment minerals as Rutile and Titanite constituents have an average of 0.188% and 0.23% respectively. Radioactive minerals as Fluorites, Zircon, and Thorite constituents have an average of 0.0075%, 0.184% and 0.001 %, respectively. Amphiboles and Pyroxene constituents range from 0.1% to 3.78% with an average of 2.22 %.

The eU contents range between 1 and 4ppm with an average 1.76ppm, while eTh is between 2 and 29ppm for with an average 10.75ppm. The average Ra average content for these sediments is 2.89ppm, and the average content of K% 1.16%.

The concentration of minerals restricted in the west (upstream) and the east (downstream) parts of the area due to the present of acidic rocks and the geomorphology of wadis. The low concentration restricted in the center part of the area where the rocks represented by basic rocks (volcanics, metavolcanics, and gabbros).

The transportation agent is rare and consid-

er seasonal so the sediment restricted near the source rock and transported short distance.

REFERENCES

- Abdel-Rahman, A.M., 1990. Petrogenesis of early-orogenic diorites, tonalites and post-orogenic trondhjemites in the Nubian shield. *J. Petrol.*, 31, 1285–1312.
- Abdel-Rahman, A.M., 1995. Tectonic–magmatic stages of shield evolution: the Pan-African belt in northeastern Egypt. *Tectonophysics*, 242, 223–240
- Akaad, M.K.; El-Gaby, S., and Habib, M.E., 1973. The Barud Gneisses and the origin of Grey Granite. *Bull. Fac. Sci. Assiut Univ.*, 2, 55–69.
- Bea, F.; Pereira, M. D.; Corretage, L. G., and Fershtater, G. B., 1994. Differentiation of strongly peraluminous, perphosphorous granites: the Pedrobenards pluton, Central Spain. *Geochemica et Cosmochemica Acta*, 58, 2609:2627.
- Bea, F., 1996. Residence of REE, Y, Th and U in granites and crustal protolith; implications for the chemistry of crustal melt. *J. Petrol.*, 37, 521:552.
- Berry, L. G.; Mason, B., and Deitrich, R. V., 1983. *Mineralogy*. Freeman, San Francisco.
- Carey, E., and Brunier, B., 1974. Analyse théorique et numérique d'un model mécanique élémentaire appliqué à l'étude d'une population de failles. *C. R. Acad. Sci. Paris*, D 279, 891-894.
- Dardir, A.A.; Khalaf, I.; Matter, E., and Aziz, M., 1987. Basement Rocks of Safajah Quadrangle, Egypt (NG36K5-6), 1:100,000 Geological Map, Egypt. *Geol. Surv. Min. Author.*, Cairo, Egypt.
- Dardir, A.A., and Abu Zeid, K.M., 1972. Geology of the basement rocks between latitudes 27_000 and 27_300N, Eastern Desert. *Ann. Geol. Surv. Egypt II*, 129–159.
- El-Akkad, S., and Dardir, A.A., 1965. Geological map of the coastal strip between Qena–Sa-

- faga road and Wadi Sharm El Bahari, scale 1:100,000 (latitudes 25_450–26_450N and longitudes 33_440–34_250E) (Noted in the list of unpublished maps of the Egyptian Geological Survey by El Ramly (1972)).
- El Gaby, S., and Habib, M. S., 1982. Geology of the area south-west of port Safaga with special emphasis on the granitic rocks, Eastern Desert, Egypt. *Ann. Geol. Surv. Egypt*, 12, 47-71.
- El-Gharbawi, R.I.A., and Hassen, I.S., 2001. The Late Precambrian metagabbro– diorite complex, Wadi Melheg area, southeastern Sinai, Egypt: an active continental margin setting. *Ann. Geol. Surv. Egypt*, XXIV, 131–158.
- El Ramly, M. F., and Akaad, M. K., 1960. The basement complex in the Central Eastern Desert of Egypt, between latitudes 24 30 and 25 40N. *Geol. Surv. Egypt. Cairo*, 8, 35p.
- El Shazly, E. M., 1964. On the classification of the Precambrian and other rocks of magmatic affiliation in Egypt. *Proc. XXII Inter. Geol. Congress, Sec.*, 10, 88-101.
- Ewing, R. C., and Haaker, R. F., 1980. The metamict state: Implications for radiation damage in crystalline waste forms. *Nuclear and Chemical Waste Management*, I, 51-57.
- Folk, R. L., and Ward, W. C., 1957. Brazos River bar: a study in the significance of grain size parameter. *J. Sedim. Petrol.*, 27, 3-27.
- Francis, M.H., 1972. Geology of the basement complex in the North Eastern Desert between latitudes 27_300 and 28_000N. *Ann. Geol. Surv. Egypt*, II, 161–180.
- Ghanem, M., 1972. Geology of the basement rocks north of latitude 28_N Eastern Desert Ras Ghareb area. *Ann. Geol. Surv. Egypt*, II, 181–197.
- Ghoneim, M.F.; Takla, M.A., and Lebda, E.M., 1992. The gabbroic rocks of the central Eastern Desert, Egypt: a geochemical approach. *Ann. Geol. Surv. Egypt*, XVIII, 1–22.
- Habib, M.S., 1970. Preliminary geological map of the area south-west of Safaga, scale 1:100,000 (latitudes 26_200–26_400N and longitudes 33_300–33_500E) (Noted in the list of unpublished maps of the Egyptian Geological Survey by El Ramly (1972)).
- Habib, M.E., 1972. Geology of the area west of Safaga, Egypt. Ph.D. Thesis, Univ. Assiut, Egypt.
- Heinrich, E. Wm., 1958. Mineralogy and geology of radioactive raw materials. McGraw-Hell Book Company, Inc., 653p.
- Hinton, R. W. and Paterson, B. A., (1994): Crystallization history of granitic magma: evidences from trace elements zoning. *Mineral. Mag.*, Vol. 58A, P. 416:417.
- Hume, W.F., 1934. Geology of Egypt II, (1) The Metamorphic Rocks, and (2) The Later Plutonic and Minor Intrusive Rocks. Government Press, Cairo.
- Ivanovich, M., 1994. Uranium series disequilibrium: concept and applications. *Radiochem. Acta*, 64, 81:94.
- Karavtchenko, G. T., 1960. Colouration of monazite. *Akad. Nauk. USSR, Sibir.*, Octdec., No. 7, 80-90.
- Masoud, M.S.; Youssef, M.M., and O'Connor, E.A., 1992. 1:250,000 Scale Geologic Map of the Al Qusayr Quadrangle, Egypt. *Egypt. Geol. Surv. Min. Author.*, Cairo, Egypt.
- Navas, A.; Soto, J., and Machin, J., 2002: ^{238}U , ^{226}Ra , ^{210}Pb , ^{232}Th and ^{40}K activities in soil profiles of the Flysch sector (Central Spanish Pyrenees). *Applied Radiation and Isotopes*. 57, 579:589.
- Pabst, A., 1952. The metamict state. *Am. Mineral.*, 37, 137:157.
- Palache, C.; Berman, H., and Frondel, C., 1944. Dana's system of mineralogy. 1, (7th edition). Wiley, New York.
- Sabet, A.H.; El-Gaby, S., and Zalata, A.A., 1972. Geology of the basement rocks in the northern parts of El-Shayib and Safaga Sheets, Eastern

- Desert. Ann. Geol. Surv. Egypt, II, 111-128.
- Speer, J. A., 1980. Zircon. In P.H. Ribble [2nd Ed.].
Reviews in Mineralogy 5: Orthosilicate Mineral Soc. Am., Washington D. C., 67-112.
- Stern, R. J., 1981. Petrogenesis and tectonic setting of late Precambrian ensimatic volcanic rocks, Central Eastern Desert of Egypt. Precambrian Res., 16, 195-230.
- Wenk, H. R., and Bulakh, A., 2004. Minerals; their constitutions and origin. Syndicate of The University of Cambridge Press.

دراسات معدنية واشعاعية لرواسب وادي ابوهمر-سفاجا-وسط الصحراء الشرقية- مصر

اشرف العزب ابراهيم

منطقة الدراسة مغطاه بصخور نارية ومتحولة ممثلة بالجابر والمتحول والبركانيات المتحولة والجرانيت القديم وبركانيات الدخان ورواسب الحمامات والجرانيت الحديث المنطقة متأثرة بخصائص تركيبية ممثلة بالصدوع المضربية تأخذ اتجاه شمال غرب وهى صدوع يمينية اما الصدوع ذات الاتجاه شرق-غرب وشمال شرق وشمال شرق بتكون صدوع يسارية اما الصدوع العادية فقد سجلت عن طريق خطوط المخدش على اسطح الصدوع المضربية. تم اخذ عدد ٤٠ عينة من الوادي ودرس التحليل الحبيبي لـ ٦٠ جرام ممثلة لكل عينة من العينات الاصلية عن طريق التقسيم مجد انها ممثلة بحجم حبيبي متوسط الى كبير وفقيرة الفرز الى متوسطة الفرز. ودرس المحتوى المعدني لهذه العينات فوجد انها تحتوى على: متوسط المعادن الثقيلة بيمثل ٤,٥% وهو يتراوح بين ٢% و ١٠,٥%. المعادن السوداء المعتمه وهى الماجنتيت والهيماتيت والالمنيت وهى تتراوح بين ١,٠٧ و ٠,١ على التوالي والمتوسط ٠,٢٨٦, اما المعادن المستخدمة فى الصنفرة مثل الجارنت فتمثل بمتوسط ٠,١٣ ومعادن المستخدمة فى البويات مثل الروتيل والتيتانيم فيمثل بمتوسط ٠,١٨٨ و ٠,٢٣ على التوالي اما المعادن المشعة فتمثل بالفلوريت والزركون والثوريت بمتوسط ٠,٠٠٧٥ و ٠,١٨٤ و ٠,٠٠١ على التوالي اما معادن الامفيبول والبيروكسين تتراوح بين ٠,١ و ٣,٧٨ بمتوسط ٢,٢٢. معادن اليورانيوم تتراوح بين ١ و ٤ جزء فى المليون بمتوسط ١,٧ جزء فى المليون بينما الثوريوم يتراوح بين ٢ و ٢٩ جزء فى المليون بمتوسط ١٠,٧٥ جزء فى المليون بينما الراديوم بمتوسط ٢,٨٩ جزء فى المليون واليوتاسيوم يمثل ١,١٦%.